Simulations of two-dimensional arrays of beads under external vibrations: Scaling behavior

S. Luding,[1] H. J. Herrmann,[2,3] and A. Blumen[1]
[1]*Theoretische Polymerphysik, Rheinstrasse 12, D-79104 Freiburg, Germany*
[2]*Höchstleistungsrechenzentrum, Kernforschungsanlage, Jülich G.m.b.H., D-52425 Jülich, Germany*
[3]*P.M.M.H., Ecole Supérieure de Physique et de Chimie Industrielles de la Ville de Paris, 10 rue Vauquelin, 75231 Paris, Cedex 05, France*
(Received 4 March 1994; revised manuscript received 24 May 1994)

We present a series of simulations on systems of beads enclosed in two-dimensional (2D) boxes, and compare the results of molecular dynamics (MD) and event-driven algorithms. The beads collide inelastically and are submitted to vibrations. We vary over a wide range the parameters: the amplitude and the frequency of the vibrations, the number of particles, and the inelasticity of the collisions. While the height of the center of mass of the system scales with respect to the restitution coefficient ϵ, the number of beads N and the typical velocity of the bottom plate, the functional dependence differs from the findings in 1D systems. We find that the MD results depend strongly on the time t_c during which the particles are in contact.

PACS number(s): 46.10.+z, 05.60.+w, 05.40.+j

I. INTRODUCTION

In recent years a lot of effort has been put into the understanding of the behavior of granular media. A recent summary of the situation has been given in Ref. [1]. Computer simulations have acquired a growing role in the understanding of basic mechanisms; an overview of presently available methods has been given in Ref. [2]. The fascinating features displayed in effects such as segregation [3–6], heap formation under vibration [7–9], as well as the formation of density waves [10] or the so-called "decompaction" in dissipative granulates [11] are due to the fact that granular media are intermediate between fluids and solids. Above a certain density a granulate is resistant to shear, while below this density the material becomes fluid. We note that the behavior of the fluid state is rather complex, especially when large fluctuations and large density gradients occur.

Fluidization may be readily observed by putting sand on a loudspeaker or on a vibrating table [7–9,12,13]. A vibrating medium conveys energy to the sand which is then dissipated through the collisions among the grains. The density of the material is, even under strongly dissipative conditions, quite reduced, so that the system can behave in many ways like a fluid. Thus under certain circumstances convection cells may appear or heaps may form spontaneously [7–9]. When particles of different sizes are put on the vibrating plate the larger ones tend to rise; this leads to a spatial segregation of the particles according to size, the larger particles coming on top.

While over the years several attempts have been made to formalize the complex rheology of granular media (here we mention kinetic theories [14,15], cellular automata methods [16], and random walk approaches [17]), computer simulations have recently evolved into playing a fundamental role. Techniques like molecular dynamics (MD) and also event-driven (ED) simulations seem particularly promising. These methods parallel other numerical methods, such as the one introduced by Cundall to study the motion of rock masses [18]: In all these approaches the granular material is seen as an assembly of discrete particles which interact at their points of contact.

Technically, ED simulations are readily visualized: Here the particles follow an undisturbed Newtonian motion as long as they are not in contact. On contact the particles conserve the overall momentum but dissipate energy, a feature which is taken care of by introducing a so-called restitution coefficient. ED algorithms were used in Refs. [19–25]. On the other hand, ED simulations based on binary collisions are hampered by the fact that at a certain threshold of energy loss the collision frequency between the particles diverges and thus clusters will form. We note that, in situations in which the particles are very often in contact, the computing time needed for ED algorithms gets to be very large. In one dimension (1D) it is possible to circumvent the problem by using the largest relative velocity (LRV) algorithm [23,24]. Here we are interested in the regime in which the particle density is low, so that the collisions are well separated in time, and we do not run into such problems.

In this work we focus on 2D situations which we analyze using both MD simulations and ED simulations, the aim being to find when the results obtained through the two methods agree. We concentrate on the fluidized regime for which (as we show) the mean height of the center of mass of the system scales with respect to the restitution coefficient, to the number of beads, and to the velocity of the bottom plate. The scaling behavior is, however, different from what is found in 1D [24].

II. SIMULATION ASPECTS

The elementary units of granular materials are mesoscopic grains, whose surface is rough on the microscopic scale. Solid friction is the immediate consequence: When

two touching grains are at rest with respect to each other a finite force F_s is needed to trigger relative motion *(static friction)*, while when the grains move against each other a finite force F_d is needed to maintain the motion *(dynamic friction)*. As a rule F_d is less than F_s; furthermore, both F_d and F_s depend only on the normal force and are independent of the relative velocity and of the area of contact (Coulomb law). Solid friction has the crucial consequence that (distinct from a situation which holds for molecular systems) on the level of the elementary units, namely, of the grains, the system does *not* conserve energy. A further source of energy dissipation is the plastic deformation of the grains, which is due to the normal forces acting during collisions.

In this work we use simple dissipation laws which, however, capture already many interesting features of the behavior of granulates. In the simulations we use N spherical particles, whose diameters are d_i $(i=1,\ldots,N)$. In some cases we pick the d_i randomly from a homogeneous distribution of width w centered at $d_0=1$ mm. In other cases we take all diameters equal; thus when we do not mention w explicitly we take it to be zero. The N particles are placed into a container of width L that is open at the top; we assume either periodic boundary conditions or fixed vertical walls.

A. Molecular dynamics method

We use a fifth order predictor-corrector MD scheme, see Ref. [25]. Let us first turn to the forces we use. Generally one has three kinds of forces acting on particle i when it overlaps with j [i.e., when the distance $r_{ij}=|\mathbf{r}_{ij}|$ is smaller than the sum of the radii $(d_i+d_j)/2$]. One has first an elastic restoration force

$$\mathbf{f}_{\rm el}^{(i)}=K[r_{ij}-\tfrac{1}{2}(d_i+d_j)]\frac{\mathbf{r}_{ij}}{r_{ij}} , \tag{1}$$

where K is the spring constant. Second, one has a dissipation force due to the inelasticity of the collision,

$$\mathbf{f}_{\rm diss}^{(i)}=-\gamma m_{ij}(\mathbf{v}_{ij}\cdot\mathbf{r}_{ij})\frac{\mathbf{r}_{ij}}{r_{ij}^2} , \tag{2}$$

where γ is a phenomenological dissipation coefficient, m_{ij} is twice the reduced mass of particles i and j, $m_{ij}=2m_im_j/(m_i+m_j)$, and $\mathbf{v}_{ij}=\mathbf{v}_i-\mathbf{v}_j$ is the relative velocity of particles i and j. Furthermore, one also has shear friction, which plays an important role in several instances (such as arching and heap formation). Here we neglect shear friction, because we are interested in situations in which the particles have long times of free flight and comparably short times of contact.

The collision of a particle with a wall is mimicked by letting the wall have infinite mass. Furthermore, the influences of gravitation and of the external vibrations are readily included: On one hand the gravitation $g=-9.81$ m/s^2 pulls each particle down; on the other hand the container is subjected to a vibrating motion described by

$$z_0(t)=A_0\sin(2\pi ft) , \tag{3}$$

where f is the frequency and A_0 the amplitude.

B. Event-driven simulations

In event-driven simulations the components of the system under analysis (here the beads) evolve independently, unless an event takes place. An event is here a collision between two particles or the collision of one particle with a wall: both situations are characterized by a sudden change of particles' momentum. Hence in ED simulations the time in which colliding particles are in contact is ideally zero. This is quite different from MD simulations, where the duration of a collision (i.e., the time t_c the beads are in contact) does not vanish, and in fact turns out to be quite significant.

In a recent work [24] numerous simulations were carried out for a 1D column of particles. For those simulations a simple event-driven algorithm was used, which updates the whole system after each event. Because of the small number of particles involved ($N\leq 100$), the procedure works quite well in 1D. The situation changes in higher dimensions, since then one also has large numbers of particles. A way to handle the matter was put forth in Ref. [22]. The advantage of the ED algorithm implemented in Ref. [22] is that one does not have to update the state of the system after each event. This is rendered possible through a double-buffering data structure where the "old" status (i.e., time, position, velocity, partner) as well as the "new" status (i.e., new time, position, velocity, partner) of each particle is recorded. If an event happens, the "new" status gets to be the "old" one and the subsequent "new" status has to be computed. This computation is performed only for the particles involved in the collision, because only their velocities changed. In the computation of the "new" status, the first step is to find the presumable new colliding partner and to calculate the "new" event time; the second step is to compute the positions and velocities after this "new" event. A "new" status might be preempted several times due to collisions of the partners with other components of the system. To make the algorithm more efficient, it is possible to apply the so-called "delayed update" method; this means to postpone examining and updating the position and the velocity of a particle until its next event; one can also store the event times in an ordered heap tree which simplifies finding the next event. For a detailed description of the algorithm see Ref. [22].

We implemented the algorithm of Ref. [22] with a few changes. First, since the calculations in [22] computed close-packed arrangements of spheres in the absence of external force fields, we included for our purposes the additional forces of gravity and of the vibrating bottom plate. Then we introduced the dissipation through the restitution coefficient for collisions, as we discuss in the following. Furthermore, we found it expedient to work with fixed sphere diameters and dispensed with the idea of dividing the container into several sectors.

For our simulations, all events which consist in collisions between two particles occur at times which can be

calculated analytically. The same holds true for collisions of the particles with the lateral walls, whereas the event times for particle collisions with the moving bottom plate have to be computed numerically . For this we use as in our 1D ED simulations [23,24] a root-finding procedure.

In the ED simulations dissipation occurs only on collision; furthermore, we let the dissipation be related to the normal component of the relative velocity only (this is the limiting case of perfectly smooth particles). The restitution coefficient ϵ thus determines the normal relative velocity after collision in the reference frame of the center of mass: $u_{ij}^{(n)}=-\epsilon v_{ij}^{(n)}$. Here $\mathbf{v}$ and $\mathbf{u}$ denote the relative velocities before and after the collision and the normal component is $v_{ij}^{(n)}=\mathbf{n}_{ij}\mathbf{v}_{ij}$ with $\mathbf{v}_{ij}=\mathbf{v}_i-\mathbf{v}_j$ and $\mathbf{n}_{ij}=\mathbf{r}_{ij}/r_{ij}$. For the restitution coefficient ϵ_w for collisions of particles with the wall one has in similar fashion $u_i^{(n)}=-\epsilon_w v_i^{(n)}$.

C. Initial conditions

In the simulations which we report we considered several initial conditions. Thus we performed simulations which started from a regular close-packing arrangement at the bottom of the container or we used as initial configuration particles randomly positioned inside a space several times higher than the height corresponding to dense packing. The initial velocities were also varied, say by setting them to zero or by picking them randomly. Before recording the values used in the averaging we let the bottom plate perform from 50 up to 1000 vibration cycles, in order to ascertain that the system is near its steady state. The displacements, velocities, and energies are then determined by averaging over up to 4000 subsequent cycles.

The simulations were carried out on a Cray Y-MP and on IBM RS6000 workstations.

III. COLLISIONS

In recent papers [23,24] a scaling behavior was reported for the position of the center of mass (c.m.) of a 1D column of beads undergoing external vibrations. In the following we will show that the corresponding scaling for 2D arrays of beads is different. In Refs. [23,24] an ED algorithm was used. The observation was that in the fluidized regime the height of the center of mass ($h_{\text{c.m.}}$) obeys

$$h_{\text{c.m.}}-h_{\text{c.m.0}}\approx[4/(3g)](A_0\omega)^2X^{-1}\ , \tag{4}$$

where $h_{\text{c.m.0}}$ is the height of the column at rest and $X=N(1-\epsilon)$ is an effective dissipation parameter. Here N denotes the number of particles and ϵ the restitution coefficient for binary collisions. In 1D N is also the number of dissipative contacts in the system.

Before utilizing MD methods, we have first to establish the connection between the parameters K and γ used in MD and the restitution coefficient ϵ used in ED simulations. We consider the collision of two particles in 1D. The situation is modeled here by a spring and a dashpot, so that setting $x''=f^{(i)}/m_i-f^{(j)}/m_j$ with $f^{(i)}=f_{\text{el}}^{(i)}+f_{\text{diss}}^{(i)}$, the following differential equation holds for the (positive) penetration depth $x=\frac{1}{2}(d_i+d_j)-r_{ij}$:

$$x''+2\gamma x'+\omega_0^2x=0\ . \tag{5}$$

In Eq. (5) one has $\omega_0=\sqrt{K/m_{\text{red}}}$ being the reduced mass $m_{\text{red}}=m_im_j/(m_i+m_j)$. The solution of Eq. (5) is

$$x(t)=(v_0/\omega)\exp(-\gamma t)\sin(\omega t)\ , \tag{6}$$

with the corresponding velocity

$$x'(t)=(v_0/\omega)\exp(-\gamma t)[-\gamma\sin(\omega t)+\omega\cos(\omega t)]\ . \tag{7}$$

In Eqs. (6) and (7) $v_0=x'(0)$ is the relative velocity before collision and $\omega=\sqrt{\omega_0^2-\gamma^2}$ a damped frequency. The contact time is given by

$$t_c=\pi/\omega \tag{8}$$

because the interaction ends when $x(t)<0$. The coefficient of restitution ϵ is defined by $\epsilon=-x'(t_c)/x'(0)$ so that

$$\epsilon=\exp(-\pi\gamma/\omega)\ . \tag{9}$$

From Eqs. (6) and (7) the maximal penetration depth $x_{\max}$ also follows; it fulfills the condition $x'(t_{\max})=0$, so that $\omega t_{\max}=\arctan(\omega/\gamma)=\arcsin(\omega/\omega_0)$ and

$$\begin{aligned}x_{\max}&=(v_0/\omega)\exp(-\gamma t_{\max})\sin(\omega t_{\max})\\&=(v_0/\omega_0)\exp[(-\gamma/\omega)\arcsin(\omega/\omega_0)]\ .\end{aligned} \tag{10}$$

For the case of low dissipation (i.e., $\omega_0\gg\gamma$) this leads to $t_{\max}=t_c/2$ and to

$$x_{\max}=v_0/\omega_0\ . \tag{11}$$

The maximal penetration depth $x_{\max}$ is in the case of, say, steel particles much smaller than the particle diameter. In our model $x_{\max}$ is proportional to v_0, see Eq. (11). In the case of high velocities (which occur for small dissipation and strong agitation) one obtains for fixed ω_0 (i.e., fixed K) rather large $x_{\max}$ values; this is a problem of the linear model underlying Eq. (5).

Now K is a function of the Young modulus and the Poisson ratio, which are material inherent and thus fix t_c for a given material. In Ref. [26] the contact time was evaluated to be $t_c\approx4.6\times10^{-6}$ s for the collision of two steel beads with diameter $d=1.5$ mm.

At low dissipation t_c is proportional to $K^{-1/2}$, see Eq. (8), so that an increase of K by a factor of 100 decreases t_c by a factor of 10. Now taking physically reasonable values for t_c leads to extremely high MD computing times. This is due to the fact that one has to ensure that several time scales of the system are well separated. Ideally one should have

$$t_{\text{MD}}\ll t_c\ll T\ , \tag{12}$$

where t_{MD} denotes the time between the simulation steps, t_c is the contact time, and $T=1/f$ is the period of the vibration. The MD simulations reported here were done with $t_{\text{MD}}<t_c/40$. We varied T in the range 0.05 s

$< T < 0.0025$ s and we used t_c values in the range 2.2×10^{-5} s $< t_c < 7\times10^{-4}$ s, by choosing K accordingly. Here we let ourselves be led by the model character of Eq. (5).

Another time variable to be aware of is the average time t_{ev} between collision events. One may approximate t_{ev} by $t_{ev}\approx l/\bar{v}$, where l is the mean free path. In 2D l is comparable to $(h_{c.m.}-h_{c.m.0})L/(Nd)$, where the quantities $h_{c.m.}$ and $h_{c.m.0}$ denote, as before, the height of the center of mass, see Eq. (4), and $\bar{v}=\langle v^2\rangle^{1/2}$ is an average velocity. We now use the quotient

$$\sigma = t_{ev}/t_c \ , \tag{13}$$

which was introduced in Refs. [26,27]. The value of σ is the ratio between the average time of free flight and the contact time t_c. For $\sigma \gg 1$ one finds almost exclusively that only pairs of particles collide. For $\sigma \ll 1$ the contact time t_c is larger than the average time between collisions. In other words, during t_c there is a high probability for a bead to interact with several others. In this case the use of the restitution coefficient ϵ to describe the energy dissipation is questionable, ϵ being defined for two-particle collisions only. In several test runs we found the condition $\sigma > 1$ to render the MD results independent of t_c. For the calculations reported here we checked that $\sigma > 2$ always holds; in fact, in most cases we even have $\sigma > 5$.

In our simulations we have as typical parameters $d_0=10^{-3}$ m, $K/m_{red}=2\times10^9$ s^{-2}, $\gamma=2\times10^3$ s^{-1}, and $t_{MD}=10^{-6}$ s. These parameters lead with the above equations to $t_c=0.7\times10^{-4}$ s, $\epsilon=0.87$ (i.e., low dissipation) and hence to $x_{max}=2.09\times10^{-5}$ m for $v_0=1$ ms^{-1} (i.e., $x_{max}=0.02d_0$). Experimentally the restitution coefficient ϵ is found to be only weakly velocity dependent; for velocities around 1 m s^{-1} one finds $\epsilon=0.6$ for aluminum and $\epsilon=0.92$ for steel [23,24]. We note here that we are allowed to use the parameters given above only for systems in which all velocities stay smaller than 1 m s^{-1}. In systems in which larger velocities occur one has to decrease the contact time to a reasonable value. As a basic finding, we note that the MD simulations lead to the same result for different values of parameters in Eqs. (1) and (2) as long as the related ϵ is the same and, most important, as long as $\sigma \gg 1$. The results from ED simulations coincide with the MD findings in this t_c range; we note that for ED calculations one has implicitly $t_c=0$.

IV. RESULTS

In the following we will discuss the behavior of N particles of diameter $d_0=10^{-3}$ m and restitution coefficient ϵ. First we let the particles fill a box of width $L=13d_0$, where in their state of lowest energy they form a triangular lattice. The height of the center of mass of this arrangement is

$$h_{c.m.0}=\frac{n_b d_0}{2N}[(1-\sqrt{3}/2)n_h+\sqrt{3}/2n_h^2] + \frac{n_0 d_0}{2N}[1+\sqrt{3}n_h] \ . \tag{14}$$

Here $n_b=L/d_0-\frac{1}{2}$ is the average number of beads per layer in the presence of walls (L/d_0 for periodic boundary conditions). In Eq. (14) $n_h=\text{entier}(N/n_b)$ is the number of full layers and $n_0=N-n_h n_b$ is the number of beads in the last layer. For $N=50$, $n_b=12.5$, and $d_0=10^{-3}$ m we find $n_h=4$ and $n_0=0$, which leads to $h_{c.m.0}=d_0/2(1+3/2\sqrt{3})=1.8\times10^{-3}$ m.

Snapshots of the system are plotted in Fig. 1(a) for different values of the dimensionless acceleration $\alpha=A_0\omega^2/g$ of the box (here $\alpha=0$, 1, 2, 5, and 10). The collision time used here was $t_c=0.7\times10^{-4}$ s. In Fig. 1(b) we plot the corresponding number-density profiles. For small α values we find that most particles are situated near the bottom of the box; the packing is dense. For large α values, the particles have long times of free flight between collisions. For the simulations in Fig. 1 we calculated σ, as given in Eq. (13), and found $\sigma=37$, 52, 74, and 120 for $\alpha=1$, 2, 5, and 10, respectively.

In the following we will analyze the behavior of the height of the center of mass $h_{c.m.}$ as a function of the parameters A_0, f, N, and ϵ, for $\sigma > 1$. At first using $N=50$ and $\epsilon=0.92$ we perform simulations in which we vary both the frequency f and the amplitude A_0 of the vibrations. Results are displayed in Fig. 2. In Fig. 2(a) we plot $h_{c.m.}-h_{c.m.0}$ as a function of α for several simulations, in which t_c varies between 7×10^{-4} s ($K/m_{red}=2\times10^7$ s^{-2}, $\gamma=118.7$ s^{-1}) and 2.2×10^{-5} s ($K/m_{red}=2\times10^{10}$ s^{-2}, $\gamma=3752$ s^{-1}). The amplitude A_0 varies from $0.1d_0$ to $6d_0$ and the frequency f varies from 20 s^{-1} up to 400 s^{-1}. The parameter sets for the symbols in Fig. 2(a) are given in Table I.

To examine the dependence of the results on size dispersion we perform two series of simulations with frequency $f=40$ s^{-1} in which we vary A_0, so that $0.08 < A_0/d_0 < 5.9$; here $L/d_0=13$ and $t_c=7\times10^{-4}$ s. As size distribution parameter we take $w=0$ (open triangles) and $w=0.05$ (filled circles). Hence for slight diameter fluctuations we observe no difference in the behavior of $h_{c.m.}$. For $\alpha > 10$ these values increase superlinearly. We connect this to the fact that for the parameters used, in this α range the maximal penetration x_{max} gets to be comparable to the radius of the particles, and thus the MD simulations no longer reproduce the behavior of metallic particles. To ascertain this statement further we present simulations (full triangles) obtained for $3.1 < A_0/d_0 < 7.0$, and $w=0$, for the same values of f and L/d_0. Contrary to the situation above we use here a much smaller contact time, $t_c=7\times10^{-5}$ s. In this case the linear regime extends to higher α values. This result is reasonable, and is supported by the fact that we find that the simulation results converge when t_c is decreased; in the following we will take care that the values of t_c used are small enough. To test that the algebraic dependence of $h_{c.m.}-h_{c.m.0}$ on α (i.e., on A_0) is not due to the particular frequency used we carried out two series of simulations in which we set $f=100$ s^{-1}; the first uses $t_c=7\times10^{-4}$ s and $0.01 < A_0/d_0 < 0.32$ (diamonds for $\alpha < 20$), the second one $t_c=7\times10^{-5}$ s and $1.25 < A_0/d_0 < 4.34$ (diamonds for $\alpha \geq 50$). Here we find

again an algebraic dependence of $h_{c.m.} - h_{c.m.0}$ on α over two orders of magnitude in α.

To find the dependence of $h_{c.m.} - h_{c.m.0}$ on the frequency f we performed three series of simulations with slightly varying A_0, so that $0.50 < A_0/d_0 < 0.63$ and varying frequency, 20 $s^{-1} < f < 141$ s^{-1}; the contact times are here 2.2×10^{-5} s $< t_c < 2.2\times10^{-4}$ s (open circles). Note the different slope of these results, which indicates that the dependence of $h_{c.m.} - h_{c.m.0}$ on f^2 is different from that on A_0 [note that f^2 is proportional to $\alpha = (A_0\omega^2)/g$].

We also performed simulations under periodic boundary conditions, by taking as repeat unit a box of width $L/d_0 = 14$. Because of this somewhat larger L value, we expect the results to change in the order of 10%. Paralleling the last simulations (open circles) we varied A_0, f, and t_c by taking $0.50 < A_0/d_0 < 0.55$ as well as 60 $s^{-1} < f < 141$ s^{-1}, and $2.2\times10^{-5} < t_c < 7\times10^{-5}$ s. The values for periodic boundary conditions (filled squares) display behaviors similar to those found for boxes with walls in this parameter range; as expected, the value of $h_{c.m.} - h_{c.m.0}$ is somewhat higher.

To look at the behavior of the system at lower amplitudes we performed for periodic boundary conditions ($L/d_0 = 14$) an additional set of simulations with $A_0/d_0 = 0.16$ and $t_c = 2.2\times10^{-4}$ s, in which we varied f in the range 40 $s^{-1} < f < 98$ s^{-1} (open squares). Finally to test the behavior of the system for extremely small amplitudes (and high frequencies) we performed a set of simulations in which we varied A_0 such as to have $5\times10^{-6} < A_0/d_0 < 10^{-4}$, while keeping fixed $f = 400$ s^{-1}, $L = 14/d_0$, and $t_c = 2.2\times10^{-4}$ s (crosses).

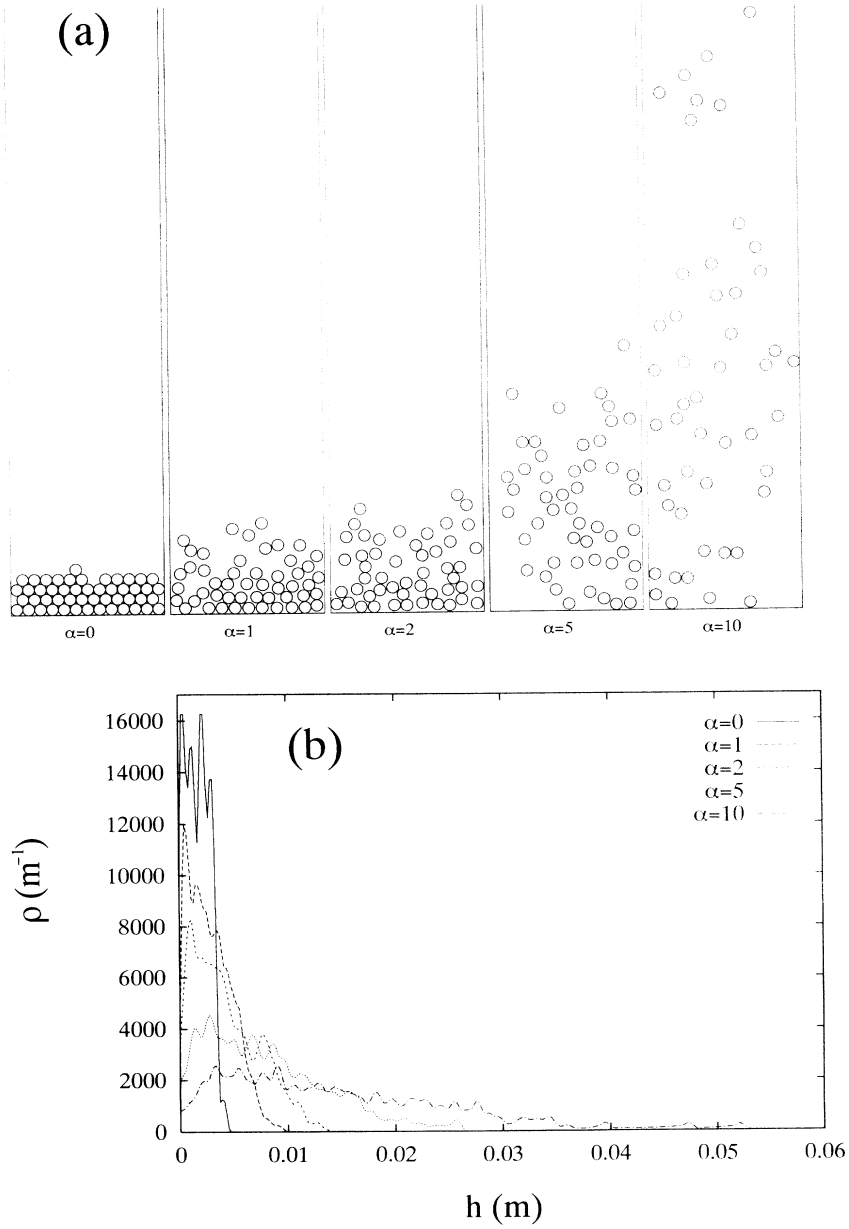

FIG. 1. (a) Typical snapshots of MD simulations. We have $N = 50$ particles in a box of width $L = 13d_0$. The parameters used are $\epsilon = 0.92$, $t_c = 0.7\times10^{-4}$ s, $f = 40$ Hz, and α varies between 0 and 10. The snapshots are taken in the steady state at phase zero. (b) Normalized density of particles ρ as function of the height h. The parameters are as in (a).

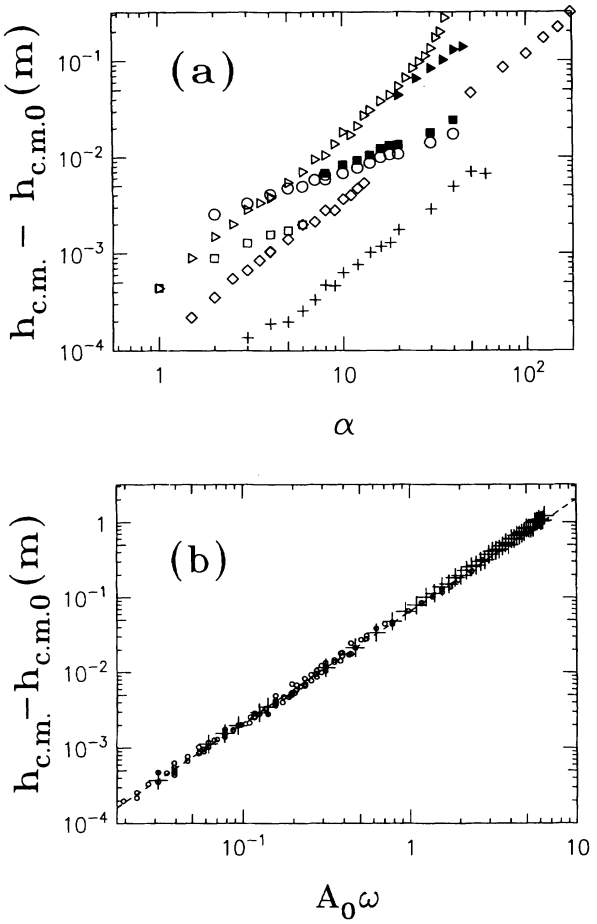

FIG. 2. (a) Log-log plot of $h_{c.m.} - h_{c.m.0}$ as a function of $\alpha = A_0\omega^2/g$ for $N = 50$ and $\epsilon = 0.92$; the parameters corresponding to the symbols are given in Table I. The averages are taken at phase zero. (b) Plotted are the values of (a) (small circles) and one series of ED simulations (crosses) as a function of $A_0\omega$. The parameters used in ED are $N = 50$, $f = 100$ s^{-1}, $\epsilon = 0.92$, $\epsilon_w = 0.96$, and $2 \leq \alpha \leq 400$. The results of (a) scale and the dashed line has the slope 1.495.

TABLE I. Parameters and symbols used in Fig. 2(a). (p) indicates periodic boundary conditions.

	A_0/d_0	f (s^{-1})	L/d_0	t_c (s)
▷	0.08 - 5.9	40	13	7x10^{-4}
●	0.08 - 5.9	40	13 w=0.05	7x10^{-4}
▶	3.1 - 7.0	40	13	7x10^{-5}
◇	0.01 - 0.32	100	13	7x10^{-4}
	1.25 - 4.34	100	13	7x10^{-5}
○	0.63	20 - 57	13	2.2x10^{-4}
	0.55	60 - 90	13	7x10^{-5}
	0.50	100 - 141	13	2.2x10^{-5}
■	0.55	60 - 90	14 (p)	7x10^{-5}
	0.50	100 - 141	14 (p)	2.2x10^{-5}
□	0.16	40 - 98	14 (p)	2.2x10^{-4}
+	5x10^{-6} - 10^{-4}	400	14 (p)	2.2x10^{-4}

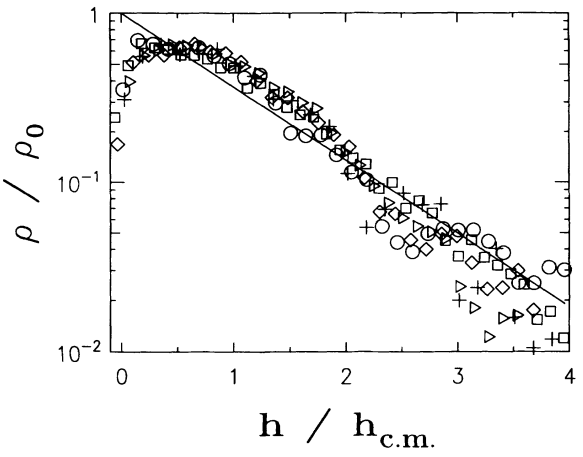

FIG. 3. Logarithmic-linear plot of the normalized number density ρ/ρ_0 for $N = 50$ and $\epsilon = 0.92$ and different f and A_0 values from Fig. 2. We use $f = 40$ s^{-1} with $A_0/d_0 = 0.93$ such that $\alpha = 6$ (squares), $A_0/d_0 = 2.17$ such that $\alpha = 14$ (diamonds), and $A_0/d_0 = 4.7$ such that $\alpha = 30$ (circles). These values correspond to the triangles of Fig. 2(a). We also use $f = 100$ s^{-1} with $A_0/d_0 = 0.5$ such that $\alpha = 20$ (triangles) and $A_0/d_0 = 1.24$ such that $\alpha = 50$ (crosses). These values correspond to the diamonds of Fig. 2(a). The straight line corresponds to $\exp(-h/h_{c.m.})$.

In Fig. 2(b) we replot the results of Fig. 2(a) (except for the values where x_{max} was found to be too large, see the discussion above). We display in logarithmic scales the dependence of $(h_{c.m.} - h_{c.m.0})$ on $A_0\omega$. We observe an impressive scaling; a linear fit leads to a slope of 1.495 ± 0.009. Within this uncertainty we can hence assert that $h_{c.m.} - h_{c.m.0} \propto (A_0\omega)^{3/2}$. Now we plot, as crosses, the result of a series of ED simulations, where we use $N = 50$ particles, $f = 100$ s^{-1}, $\epsilon = 0.92$, $\epsilon_w = 0.96$ and we vary α in the range $2 \leq \alpha \leq 400$. As is obvious from the figure the ED simulations lead to the same results as the MD simulations.

In Fig. 3 we plotted the number-density profiles $\rho(h)$ for different α values, $6 < \alpha < 50$. We scale now the results by displaying the height h in units of $h_{c.m.}$ and the number density in units of $\rho_0 = 1/h_{c.m.}$. For comparison we also give the exponential function $\exp(-h/h_{c.m.})$, represented as a straight line. This exponential form is the density profile of a Boltzmann gas without dissipation. From Figs. 2 and 3 we find that in the fluidized regime the height of the center of mass (and thus the potential energy) scales with the typical velocity $A_0\omega$ [or energy $(A_0\omega)^2/2$] of the box and not with the acceleration α. This situation parallels our finding [24] in the 1D case. Also the density profiles for different amplitudes and frequencies scale with $A_0\omega$ (i.e., $h_{c.m.}$). We attribute to the dissipative aspect of the collisions the fact that in our model the density profiles differ from the Boltzmann-gas behavior.

In the following we will discuss the dependence of $h_{c.m.}$ on N and ϵ, the parameters which control dissipation. In Fig. 4(a) we plot $h_{c.m.} - h_{c.m.0}$ as a function of $X = (N/n_b)(1-\epsilon)$. This definition is consistent with the

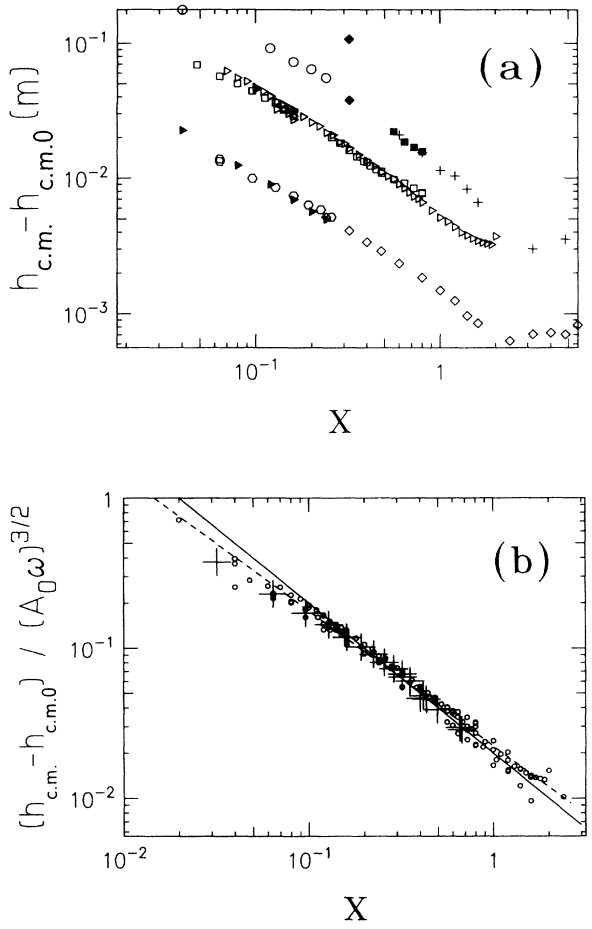

FIG. 4. (a) Log-log plot of $h_{c.m.}-h_{c.m.0}$ as a function of $X=(N/n_b)(1-\epsilon)$ in a box of width $L=13d_0$; the parameters corresponding to the symbols are shown in Table II. The averages are taken at phase zero. (b) Plotted are the results of (a) (small circles) and a series of ED simulations (crosses), scaled by $(A_0\omega)^{3/2}$, as a function of X. The parameters used in ED are $\alpha=10$ and 50, $f=100\ s^{-1}$, $\epsilon=0.96$, $\epsilon_w=0.98$, and $10\le N\le 205$. The dashed line has the slope -0.90, the full line the slope -1. We find again an impressive coincidence of ED and MD results.

TABLE II. Parameters and symbols used in Fig. 4(a).

	N	ε	α	$f(s^{-1})$	t_c (s)
▷	50	0.5 - 0.9825	10	40	7×10^{-5} - 7×10^{-4}
▶	50	0.94 - 0.99	10	100	7×10^{-5}
○	50	0.7 - 0.925	50	100	7×10^{-5}
◇	100	0.2 - 0.97	10	100	7×10^{-5}
+	100	0.2 - 0.925	50	100	7×10^{-5}
□	15-250	0.96	10	40	7×10^{-5} - 7×10^{-4}
⬡	40-160	0.98	10	100	3×10^{-5}
■	175-250	0.9	50	100	7×10^{-5} - 7×10^{-4}
◆	100 200 400	0.96 0.98 0.99	100 100 50	100 100 100	7×10^{-5}

1D case, in which $n_b=1$, so that in 1D one has, as before, $X=N(1-\epsilon)$.

In the simulations displayed in Fig. 4(a) we use $L=13d_0$ (no periodic boundary conditions), the other parameters can be extracted from Table II.

To find the behavior of the system for different ϵ values we first carry out three series of simulations, in which we set $N=50$ and scan ϵ in the range $0.5<\epsilon<0.99$. Here we use $f=40\ s^{-1}$ and $\alpha=10$ (open triangles), $f=100\ s^{-1}$ and $\alpha=10$ (filled triangles), as well as $f=100\ s^{-1}$ and $\alpha=50$ (circles); t_c is taken in the range $7\times10^{-5}\ s<t_c<7\times10^{-4}\ s$. In general we find that $h_{c.m.}-h_{c.m.0}$ decreases with increasing X (i.e., with decreasing ϵ).

Furthermore, in two more sets of simulations we keep $N=100$ fixed and scan ϵ in the range $0.2<\epsilon<0.97$. We take here $t_c=7\times10^{-5}$ s, $f=100\ s^{-1}$, and choose $\alpha=10$ (results indicated by diamonds) and $\alpha=50$ (results indicated by crosses). The outcome of this set of simulations is that for $X>2$ (i.e., $\epsilon<0.5$) the values no longer follow an algebraic behavior; in this X range the fluctuations of $h_{c.m.}-h_{c.m.0}$ are much larger than for $X<2$. The system here is close to dense packing and we are thus quite far from the fluidized regime.

To test the behavior of the system when the number of particles changes, we vary N in the range $15<N<250$ and use ϵ values in the range $0.9<\epsilon<0.98$; furthermore, we take $f=40\ s^{-1}$ and $\alpha=10$ (open squares), $f=100\ s^{-1}$ and $\alpha=10$ (hexagons), as well as $f=100\ s^{-1}$ and $\alpha=50$ (filled squares), while t_c varies in the interval $3\times10^{-5}\ s<t_c<7\times10^{-4}\ s$. Here we again find that $h_{c.m.}-h_{c.m.0}$ decreases with increasing X (i.e., with increasing N).

In Fig. 4(b) we plot on the vertical axis $(h_{c.m.}-h_{c.m.0})/(A_0\omega)^{3/2}$ as a function of X and the results scale again. The best linear fit gives the slope -0.90 ± 0.01; also, as indicated in Fig. 4(b), a value of -1 is still acceptable. Hence in the sense of simplicity we have $h_{c.m.}-h_{c.m.0}\propto 1/X$. We tested for several pa-

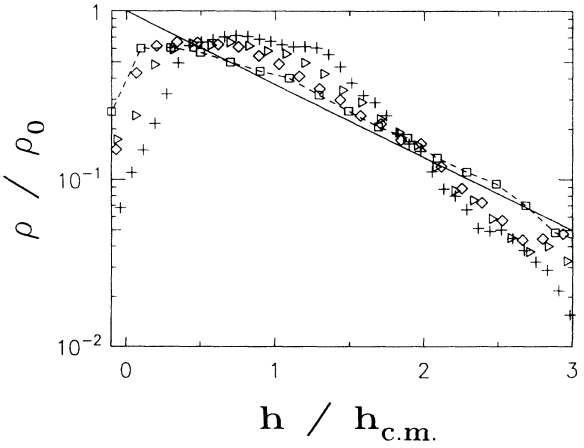

FIG. 5. Logarithmic-linear plot of the normalized number density ρ/ρ_0 for $N=50$, $A_0=1.55d_0$, and $f=40$ Hz, such that $\alpha=10$. Here ϵ equals 0.6 (crosses), 0.8 (triangles), 0.9 (diamonds), and 0.95 (squares, connected by dashed lines). These simulations correspond to the triangles of Fig. 4(a). The straight line corresponds to $\exp(-h/h_{c.m.})$.

rameters that the height of the center of mass does not change much with decreasing t_c. We carried out a series of ED simulations, where we used $f=100\ s^{-1}$, $\alpha=10$ and 50, $\epsilon=0.96$, and $\epsilon_w=0.98$, while we varied N in the range $10\leq N\leq 205$. These results are plotted as crosses in Fig. 4(b); we again find that the ED and MD simulations lead to impressive agreement. We attribute the deviations from the X^{-1} behavior for small X values mainly to the dissipative collisions with the walls.

In Fig. 5 we plot the density profiles for $N=50$, $f=40\ s^{-1}$, and $\alpha=10$, while we vary ϵ between 0.6 and 0.95. The normalized density profiles tend to an exponential function when ϵ tends towards unity. In other words, if the dissipation is low (small X) the density profiles are of nearly exponential form, whereas for large X values deviations occur: the particles concentrate in a middle position, and the system is less spread out.

V. SUMMARY AND CONCLUSION

From a methodological point of view our work shows that the results of MD and ED simulations agree with each other in the fluidized regime. A good condition for this agreement is $\sigma \gg 1$. In Refs. [23,24] we have compared ED-simulation results obtained through our algorithm with 1D experiments, and we found a very good agreement. Our present results show that we can trust the MD simulations for $\sigma \gg 1$ as well. Interestingly, for $\sigma < 1$, the ED and the MD findings may differ strongly [26]. Hence it is extremely important to compare the results to experimental findings, in order to assess the range of validity of the methods. From the computational point of view ED simulations are very effective in the fluidized regime, while MD simulations perform better when the particle density is high.

On a more technical note, we find both from ED and MD calculations that the height of the center of mass for a 2D assembly of inelastic spheres scales. We obtain

$$h_{\text{c.m.}}-h_{\text{c.m.0}}\approx C(A_0\omega)^{3/2}[(N/n_b)(1-\epsilon)]^{-1} = C(A_0\omega)^{3/2}/X\ , \tag{15}$$

with $C=0.02\ s^{3/2}\,m^{-1/2}$. We recall that scaling was also found in 1D [24], see Eq. (4); also in Eq. (4) the basic parameters are $A_0\omega$ and X. In particular, as already asserted in Ref. [28], $h_{\text{c.m.}}-h_{\text{c.m.0}}$ does not depend on the acceleration, although the onset of fluidization does [8]. A difference consists in the fact that here, in 2D, the power law of $A_0\omega$ is $\frac{3}{2}$, whereas it is 2 in 1D. On the other hand, the dependence on X is the same in 1D and in 2D. In 1D the exponent of X was found to be -1 for $X<0.1$ (for $0.1<X<2.8$ a second order polynomial correction for the X dependence was applied), while in 2D we find the exponent of X to be around -1 in the range $0.05<X<2$.

Possible extensions of the algorithms used here may include static and dynamic friction, the rotations of particles, and variations in the particles' shapes. Another restriction of our algorithms is their 2D aspect; we note that the extension of our techniques to 3D is now in progress. In 1D and in 2D we encounter the same fundamental problem: one has to be aware of the different time scales, t_c, t_{ev}, and T, which arise in the system and of the difficulties which may occur if these time scales are not well separated.

ACKNOWLEDGMENTS

The support of the Deutsche Forschungsgemeinschaft (SFB 60), of the Fonds der Chemischen Industrie, and of the HLRZ-Jülich (grant of Cray computing time) is gratefully acknowledged.

[1] *Disorder and Granular Media,* edited by D. Bideau and A. Hansen (Elsevier, Amsterdam, 1993).

[2] H. J. Herrmann, in *Disorder and Granular Media,* edited by D. Bideau and A. Hansen (Elsevier, Amsterdam, 1993), pp. 305–320.

[3] J. C. Williams, Powder Technol. **15**, 245 (1976).

[4] A. Rosato, K. J. Strandburg, F. Prinz, and R. H. Swendsen, Phys. Rev. Lett. **58**, 1038 (1987); Powder Technol. **49**, 59 (1986); P. Devillard, J. Phys. (Paris) **51**, 369 (1990); R. Jullien, P. Meakin, and A. Pavlovitch, Phys. Rev. Lett. **69**, 640 (1992).

[5] P. K. Haff and B. T. Werner, Powder Technol. **48**, 239 (1986).

[6] J. Duran, J. Rajchenbach, and E. Clément, Phys. Rev. Lett. **70**, 2431 (1993).

[7] M. Faraday, Philos. Trans. R. Soc. London **52**, 299 (1831).

[8] P. Evesque and J. Rajchenbach, Phys. Rev. Lett. **62**, 44 (1989); C. R. Acad. Sci. Ser. B **307**, 1 (1988); **307**, 223 (1988); C. Laroche, S. Douady, and S. Fauve, J. Phys. (Paris) **50**, 699 (1989); S. Douady, S. Fauve, and C. Laroche, Europhys. Lett. **8**, 621 (1989); P. Evesque, J. Phys. (Paris) **51**, 697 (1990); J. Rajchenbach, Europhys. Lett. **16**, 149 (1991); E. Clément, J. Duran, and J. Rajchenbach, Phys. Rev. Lett. **69**, 1189 (1992).

[9] J. Walker, Sci. Am. **247**, 167 (1982); F. Dinkelacker, A. Hübler, and E. Lüscher, Biol. Cybern. **56**, 51 (1987).

[10] G. W. Baxter, R. P. Behringer, T. Fagert, and G. A. Johnson, Phys. Rev. Lett. **62**, 2825 (1989); P. C. Johnson and R. Jackson, J. Fluid Mech. **176**, 67 (1987).

[11] J. Duran, T. Mazozi, E. Clément, and J. Rajchenbach, Phys. Rev. E **50**, 3092 (1994).

[12] E. Clément and J. Rajchenbach, Europhys. Lett. **16**, 133 (1991).

[13] P. Evesque, E. Szmatula, and J.-P. Denis, Europhys. Lett. **12**, 623 (1990); O. Zik and Stavans, *ibid.* **16**, 255 (1991); O. Zik, J. Stavans, and Y. Rabin, *ibid.* **17**, 315 (1992).

[14] S. B. Savage, Adv. Appl. Mech. **24**, 289 (1984); C. S. Campbell, Annu. Rev. Fluid Mech. **22**, 57 (1990).

[15] S. B. Savage, J. Fluid Mech. **92**, 53 (1979); G. M. Homsy, R. Jackson, and J. R. Grace, *ibid.* **236**, 477 (1992); S. B. Savage and K. Hutter, *ibid.* **199**, 177 (1989); P. K. Haff, *ibid.* **134**, 401 (1983); J. T. Jenkins and M. W. Richman,

Arch. Rat. Mech. Anal. **87**, 355 (1985).
[16] G. W. Baxter and R. P. Behringer, Phys. Rev. A **42**, 1017 (1990); Physica D **51**, 465 (1991).
[17] H. Caram and D. C. Hong, Phys. Rev. Lett. **67**, 828 (1991).
[18] P. A. Cundall, Report No. AD/A-001 602 (U.S. National Technical Information Service, Springfield, VA, 1974); P. A. Cundall and O. D. L. Strack, Géotechnique **29**, 47 (1979).
[19] S. McNamara and W. R. Young, Phys. Fluids A **4**, 496 (1992).
[20] S. McNamara and W. R. Young, Phys. Fluids A **5**, 34 (1993).
[21] B. Bernu and R. Mazighi, J. Phys. A **23**, 5745 (1990).
[22] B. D. Lubachevsky, J. Comput. Phys. **94**, 255 (1991).
[23] E. Clément, S. Luding, A. Blumen, J. Rajchenbach, and J. Duran, Int. J. Mod. Phys. B **7**, 1807 (1993).
[24] S. Luding, E. Clément, A. Blumen, J. Rajchenbach, and J. Duran, Phys. Rev. E **49**, 1634 (1994).
[25] M. P. Allen and D. J. Tildesley, *Computer Simulation of Liquids* (Oxford University Press, Oxford, 1987).
[26] S. Luding, E. Clément, A. Blumen, J. Rajchenbach, and J. Duran, Phys. Rev. E **50**, (to be published).
[27] S. Luding, E. Clément, A. Blumen, J. Rajchenbach, and J. Duran, Phys. Rev. E **50**, 1762 (1994).
[28] J. A. C. Gallas, H. J. Herrmann, and S. Sokołowski, Physica A **189**, 437 (1992); J. A. C. Gallas, H. J. Herrmann, and S. Sokołowski, Phys. Rev. Lett. **69**, 1371 (1992).